Nonlinearities in the Response of Beam Position Monitors for the LEP Spectrometer

John Matheson

CERN, CH-1211 Geneva 23, Switzerland

March 5, 2001

Abstract

The LEP Spectrometer determines the energy of the beam by measuring the bending angle due to a dipole magnet, using a total of six beam position monitors (BPM). The response to an off-center beam of a BPM is not strictly linear with displacement and, in addition, depends on the size of the beam. The response also depends on the shape of the aperture of the BPM itself, since the inner surface is conducting and must therefore be an equipotential. For the LEP Spectrometer, BPM nonlinearities may become large enough to affect the beam energy measurement. We calculate the size of the effect for Gaussian beams within circular and elliptical apertures, drawing conclusions regarding the operation of the Spectrometer.

1 Introduction

The Large Electron-Positron (LEP) collider at CERN has been used to study decays of W bosons since 1996. To produce a W^+W^- pair requires a centre of mass energy of 160.6 GeV and the goal of 100 GeV per beam was surpassed during the 1999 LEP running period. For precise determination of the W mass, the target for beam energy calibration is to reduce the uncertainty to below ± 30 MeV in the centre of mass frame.

Up to 60 GeV at LEP, the technique of resonant spin depolarisation has been used to calibrate the beam energy [1]; this is the most accurate technique available. However, as the beam energy is increased, imperfections in the vertical orbit cause depolarising effects and a polarisation level sufficient for the measurement cannot be achieved. For this reason, beam energy information is derived by sampling the bending magnetic field of LEP up to the physics energies.

The sampling of the bending field is carried out by means of a flux loop and nuclear magnetic resonance (NMR) probes [2]. However, the accuracy of the measurement is limited by the fact that only part of the total bending field is covered. Hence the LEP Spectrometer [3] was proposed with the intention of being an alternative method of energy determination.

The Spectrometer consists of a laminated steel dipole magnet equipped with reference NMR probes. At each side of the magnet, the beam pipe is instrumented with three BPM stations for the reconstruction of the bending angle of the beam (Fig. 1). The integral field of the magnet has been determined as a function of the reference probe readings with a relative accuracy of 3×10^{-5} [4]. As the energy of the beams is ramped, the current through the magnet is ramped also, to keep the bending angle constant. The purpose of the BPMs, then, is to monitor changes in the angle. The Spectrometer is also calibrated at low energy against resonant depolarisation, providing a relative energy measurement after the ramp to the physics energy. Thus, the need for an absolute measurement of the deflection is avoided. The accuracy required of the Spectrometer is $\delta E/E < 1 \times 10^{-4}$. The same accuracy is required for the monitoring of deviations from the nominal bending angle, which in turn implies $\pm 1\,\mu$m BPM resolution.

Each BPM consists of four 34 mm diameter stainless steel button electrodes mounted in an aluminium block, the aperture of which is elliptical. The horizontal axis of the ellipse is 131mm and the vertical axis is 70mm (Fig. 2). The passage of a beam bunch induces a signal on each electrode, depending in magnitude on the distance between the beam and that electrode. The induced signal on a single electrode is also proportional to the bunch current and the signals from all four electrodes are used to allow normalisation. The pickup electronics were custom manufactured for the Spectrometer application, based on a design for synchrotron light sources, with a specification of $\sim 1\,\mu$m resolution [5].

It has been shown that the beam size affects the response of BPMs based on striplines which sense wall current in the beam pipe [6], the wall current being proportional the induced charge at the pipe surface.

The beam size effect is identical for a capacitive pickup electrode such as that used in the Spectrometer application, since such an electrode also responds to the induced charge. The induced charge depends on the component of the electric field normal to the pipe surface; the charge distribution must be such that the conducting pipe is rendered an equipotential surface. Hence, the BPM response will depend on the shape of the pipe as well as the characteristics of the pickup electrodes.

We derive analytically the beam size effect for a round pipe, finding a difference between our result and that cited in [6]. The analysis suggests naturally a method for numerical simulation of the BPM response, which we have applied to the case of a round pipe and to that of an elliptical pipe. The behaviour of the BPM in the elliptical geometry allows conclusions to be drawn regarding effects on the Spectrometer arising from nonlinearities in pickup response.

2 Analytical response of a circular BPM

2.1 Image charge for a circular pipe

For an ultra-relativistic beam of charged particles in a vacuum chamber, the current density induced on the inner surface of the vessel may be approximated, in the low frequency limit, by that due to a line charge at the beam position [7]. This induced charge may be calculated by the method of images. Placing an infinite line charge at some point within the pipe, we search for the distribution of image charges outside the pipe which will result in the pipe itself being an equipotential.

For certain pipe shapes, it is possible to find a conformal mapping, such that the pipe may be represented in a simpler geometry. For a circular pipe, we draw a circle radius a, centre $(0, ia)$ in the complex plane $Z = x + iy$ [8]. The function:

$$W = \frac{1}{Z} + \frac{i}{2R} \tag{1}$$

maps the circle to the u axis in the complex plane $W = u + iv$ (Fig. 3). Then, if an infinite line charge λ is placed within the plane Z at the point:

$$Z_{beam} = (0, ir) \tag{2}$$

it will appear in the plane W at the point:

$$W_{beam} \;=\; \left(0, -i\frac{a-r}{2a(r+a)}\right) \tag{3}$$

One can see immediately that the image charge necessary to make the u axis an equipotential is a charge of $-\lambda$ at:

$$W_{image} \;=\; \left(0, +i\frac{a-r}{2a(r+a)}\right) \tag{4}$$

Transforming this image charge position back from W into Z using:

$$Z = \frac{1}{(W - i/2a)} \tag{5}$$

yields the image in Z at:

$$Z_{image} \;=\; \left(0, i\left(a + \frac{a^2}{r}\right)\right) \tag{6}$$

that is, at a distance a^2/r from the centre of the circle.

2.2 Field due to a line charge within a circular pipe

The field at any point on the pipe may be obtained by adding up the fields due to the line charge "beam" and its image. The induced charge at the beam pipe is due to the component of the field normal to the surface. This situation is depicted in Fig. 4; due to the beam, the normal component of the field observed at the point P is:

$$E_{beam} \;=\; \frac{\lambda}{2\pi\epsilon_0 d_1}\cos\alpha \;=\; \frac{\lambda}{2\pi\epsilon_0 d_1}\cdot\frac{a - r\cos\theta}{d_1} \tag{7}$$

where λ is the charge per unit length of the beam. Let γ be the angle between the line d_2 and the radius passing through P:

$$\gamma \;=\; \pi - (\theta + \beta) \quad\Rightarrow\quad \cos\gamma \;=\; \sin\theta\sin\beta \;-\; \cos\theta\cos\beta \tag{8}$$

Since we have:

$$\sin\beta \;=\; \frac{a\sin\theta}{d_2} \quad , \quad \cos\beta \;=\; \frac{a^2/r - a\cos\theta}{d_2} \tag{9}$$

the field at P normal to the surface and due to the image charge becomes:

$$E_{image} \;=\; -\frac{\lambda}{2\pi\epsilon_0 d_2}\cos\gamma \;=\; -\frac{\lambda}{2\pi\epsilon_0 d_2}\cdot\frac{a - (a^2/r)\cos\theta}{d_2} \tag{10}$$

Thus, the total field in the normal direction is:

$$E_{total} \;=\; E_{beam} + E_{image} \;=\; \frac{\lambda}{2\pi\epsilon_0}\left(\frac{a - r\cos\theta}{d_1^2} - \frac{a - (a^2/r)\cos\theta}{d_2^2}\right) \tag{11}$$

We may substitute for d_1^2 and d_2^2 explicitly as:

$$d_1^2 \;=\; a^2 + R^2 - 2ar\cos\theta \quad , \quad d_2^2 \;=\; a^2 + a^4/r^2 - (2a^3/r)\cos\theta \tag{12}$$

After some rearrangement, we obtain the result:

$$E_{total} \;=\; E_\lambda \frac{a^2 \;-\; r^2}{a^2 + r^2 - 2ar\cos(\theta - \phi)} \tag{13}$$

where $E_\lambda \;=\; \lambda/2\pi\epsilon_0 a$ is the field at radius a in the absence of the pipe. We have generalised the expression to treat a beam which lies away from the x axis, at a position (r, ϕ) in cylindrical polar coordinates, by rotating Fig. 4 through an angle ϕ about the centre of the circle.

Since the density of the current flowing on the pipe wall at any angle θ is proportional to the field at that point, we may also write:

$$J \;=\; \left(\frac{I}{2\pi a}\right)\frac{a^2 \;-\; r^2}{a^2 + r^2 - 2ar\cos(\theta - \phi)} \tag{14}$$

where J is the current density and I is the total beam current. This result is given without derivation in [6] and [9].

2.3 Response of a circular BPM to a line charge

We may calculate the response of a BPM by first expanding (13) in a power series according to the result [10]:

$$1 + 2\sum_{k=1}^{\infty} p^k \cos kx \;=\; \frac{1 \;-\; p^2}{1 - 2p\cos x + p^2} \tag{15}$$

from which we obtain after some substitution:

$$E \;=\; E_\lambda \left[1 + 2\sum_{k=1}^{\infty}\left(\frac{r}{a}\right)^k \cos k(\theta - \phi)\right] \tag{16}$$

Writing out the series explicitly:

$$\sum_{k=1}^{\infty}\left(\frac{r}{a}\right)^k \cos k(\theta - \phi) \approx \frac{r}{a}\cos(\theta - \phi) + \frac{r^2}{a^2}\cos 2(\theta - \phi) + \frac{r^3}{a^3}\cos 3(\theta - \phi) \tag{17}$$

By means of standard trigonometric identities and by writing $\cos\phi = x/r$ and $\sin\phi = y/r$, it may be shown that:

$$\cos(\theta - \phi) = \frac{x}{r}\cos\theta + \frac{y}{r}\sin\theta \tag{18}$$

$$\cos 2(\theta - \phi) = \left(\frac{x^2}{r^2} - \frac{y^2}{r^2}\right)\cos 2\theta + \frac{2xy}{r^2}\sin 2\theta \tag{19}$$

$$\cos 3(\theta - \phi) = \left(\frac{x^3}{r^3} - \frac{3xy^2}{r^3}\right)\cos 3\theta - \left(\frac{y^3}{r^3} - \frac{3x^2y}{r^3}\right)\sin 3\theta \tag{20}$$

Thus, the field in the radial direction at a given angle may be approximated as:

$$\begin{aligned} E \approx E_\lambda\{1 + 2\,[\frac{x}{a}\cos\theta \quad &+ \quad \frac{y}{a}\sin\theta + \left(\frac{x^2}{a^2} - \frac{y^2}{a^2}\right)\cos 2\theta + \frac{2xy}{a^2}\sin 2\theta \\ &+ \quad \left(\frac{x^3}{a^3} - \frac{3xy^2}{a^3}\right)\cos 3\theta - \left(\frac{y^3}{a^3} - \frac{3x^2y}{a^3}\right)\sin 3\theta\,]\} \end{aligned} \tag{21}$$

If the BPM buttons are sufficiently small that they may be represented by points at their centres, the signal from each button may be calculated simply. Considering buttons at angles $\pi/4$, $3\pi/4$, $5\pi/4$ and $7\pi/4$ from the x-axis we have:

$$E_{\pi/4} \approx \left(\frac{I}{2\pi a}\right)\left\{1 + 2\left[\frac{x}{a\sqrt{2}} + \frac{y}{a\sqrt{2}} + \frac{2xy}{a^2} - \frac{1}{\sqrt{2}}\left(\frac{x^3 - 3xy^2}{a^3}\right) - \frac{1}{\sqrt{2}}\left(\frac{y^3 - 3x^2y}{a^3}\right)\right]\right\} \tag{22}$$

$$E_{3\pi/4} \approx \left(\frac{I}{2\pi a}\right)\left\{1 + 2\left[-\frac{x}{a\sqrt{2}} + \frac{y}{a\sqrt{2}} - \frac{2xy}{a^2} + \frac{1}{\sqrt{2}}\left(\frac{x^3 - 3xy^2}{a^3}\right) - \frac{1}{\sqrt{2}}\left(\frac{y^3 - 3x^2y}{a^3}\right)\right]\right\} \tag{23}$$

$$E_{5\pi/4} \approx \left(\frac{I}{2\pi a}\right)\left\{1 + 2\left[-\frac{x}{a\sqrt{2}} - \frac{y}{a\sqrt{2}} + \frac{2xy}{a^2} + \frac{1}{\sqrt{2}}\left(\frac{x^3 - 3xy^2}{a^3}\right) + \frac{1}{\sqrt{2}}\left(\frac{y^3 - 3x^2y}{a^3}\right)\right]\right\} \tag{24}$$

$$E_{7\pi/4} \approx \left(\frac{I}{2\pi a}\right)\left\{1 + 2\left[\frac{x}{a\sqrt{2}} - \frac{y}{a\sqrt{2}} - \frac{2xy}{a^2} - \frac{1}{\sqrt{2}}\left(\frac{x^3 - 3xy^2}{a^3}\right) + \frac{1}{\sqrt{2}}\left(\frac{y^3 - 3x^2y}{a^3}\right)\right]\right\} \tag{25}$$

A typical algorithm used by BPM readout electronics to give signals representing horizontal and vertical beam displacements is:

$$\Delta_X = \frac{(S1 - S3) - (S2 - S4)}{(S1 + S2 + S3 + S4)} \tag{26}$$

$$\Delta_Y = \frac{(S1 - S3) + (S2 - S4)}{(S1 + S2 + S3 + S4)} \tag{27}$$

where $S1$ to $S4$ denote the button signals in order of increasing angle (see Fig. 2). The button signals are proportional to the field normal to the pipe, whether stripline or capacitive sensing is employed. Substituting for the individual button signals, we obtain:

$$\Delta_X = \sqrt{2}\,\frac{x}{a}\left[1 - \left(\frac{x^2 - 3y^2}{a^2}\right)\right] \tag{28}$$

$$\Delta_Y = \sqrt{2}\,\frac{y}{a}\left[1 - \left(\frac{y^2 - 3x^2}{a^2}\right)\right] \tag{29}$$

which predicts a response which departs increasingly from linearity as the beam displacements increase. For small displacements, a linear approximation may suffice and it is common to take $x = K_H \Delta_X$ and $y = K_V \Delta_Y$, where K_H and K_V are constants. For our simplified model with point buttons, $K_H = K_V = a/\sqrt{2}$, but in reality K_H and K_V will depend on the precise electrode geometry.

2.4 Response of a circular BPM to a Gaussian beam

To take into account the distribution of line charges within a real beam, the line charge density λ may be multiplied by a suitable weighting function. Then the induced charge at any point on the beam pipe must be calculated by integrating over all the individual charges at positions (x, y) within the beam. For Gaussian beam distributions in both transverse directions, the field normal to the pipe becomes from (16):

$$\begin{aligned} E &= \frac{E_\lambda}{2\pi\sigma_x\sigma_y}\int_{-\infty}^{\infty}\int_{-\infty}^{\infty}\left[1 + 2\sum_{k=1}^{\infty}\left(\frac{r}{a}\right)^k \cos k(\theta - \phi)\right] \\ &\qquad \times\ \exp -\left[\frac{(x-\bar{x})^2}{2\sigma_x^2}\right]\exp -\left[\frac{(y-\bar{y})^2}{2\sigma_y^2}\right]\,dx\ dy \end{aligned} \tag{30}$$

where the integration over the beam area has been approximated by integration over all space. The parameters $\bar{x}$ and $\bar{y}$ represent the mean position of the beam and σ_x and σ_y the standard deviations in the x and y directions. The integration may be performed after writing out the series explicitly as before. We denote the individual terms by writing $E \approx E_0 + E_1 + E_2 + E_3$ and integrate term by term:

$$E_0 = \frac{E_\lambda}{2\pi\sigma_x\sigma_y}\int\int \exp -\left[\frac{(x-\bar{x})^2}{2\sigma_x^2}\right]\exp -\left[\frac{(y-\bar{y})^2}{2\sigma_y^2}\right]\,dx\ dy \tag{31}$$

$$E_1 = \frac{E_\lambda}{2\pi\sigma_x\sigma_y}\int\int 2\left(\frac{x}{a}\cos\theta + \frac{y}{a}\sin\theta\right)\ \exp -\left[\frac{(x-\bar{x})^2}{2\sigma_x^2}\right]\exp -\left[\frac{(y-\bar{y})^2}{2\sigma_y^2}\right]\,dx\ dy \tag{32}$$

$$E_2 = \frac{E_\lambda}{2\pi\sigma_x\sigma_y}\int\int 2\left[\left(\frac{x^2}{a^2}-\frac{y^2}{a^2}\right)\cos 2\theta + \frac{2xy}{a^2}\sin 2\theta\right]$$
$$\times \exp - \left[\frac{(x-\bar{x})^2}{2\sigma_x^2}\right] \exp - \left[\frac{(y-\bar{y})^2}{2\sigma_y^2}\right] dx\ dy \tag{33}$$

$$E_3 = \frac{E_\lambda}{2\pi\sigma_x\sigma_y}\int\int 2\left[\left(\frac{x^3}{a^3}-\frac{3xy^2}{a^3}\right)\cos 3\theta - \left(\frac{y^3}{a^3}-\frac{3x^2y}{a^3}\right)\sin 3\theta\right]$$
$$\times \exp - \left[\frac{(x-\bar{x})^2}{2\sigma_x^2}\right] \exp - \left[\frac{(y-\bar{y})^2}{2\sigma_y^2}\right] dx\ dy \tag{34}$$

The integrals may be performed using the following results [11]:

$$\int_{-\infty}^{\infty}\left(\frac{1}{b}\right) exp- \left[\frac{(u-a)^2}{2b^2}\right] du = \sqrt{2\pi} \quad , \quad \int_{-\infty}^{\infty}\left(\frac{u}{b}\right) exp- \left[\frac{(u-a)^2}{2b^2}\right] du = \sqrt{2\pi}\,(a) \tag{35}$$

$$\int_{-\infty}^{\infty}\left(\frac{u^2}{b}\right) exp- \left[\frac{(u-a)^2}{2b^2}\right] du = \sqrt{2\pi}(a^2+b^2) \tag{36}$$

$$\int_{-\infty}^{\infty}\left(\frac{u^3}{b}\right) exp- \left[\frac{(u-a)^2}{2b^2}\right] du = \sqrt{2\pi}(a^3+3ab^2) \tag{37}$$

Integrating each term, we find:

$$E \approx E_\lambda \{1 + 2\,[\frac{\bar{x}}{a}\cos\theta + \frac{\bar{y}}{a}\sin\theta + \left(\frac{{\sigma_x}^2-{\sigma_y}^2}{a^2}+\frac{\bar{x}^2-\bar{y}^2}{a^2}\right)\cos 2\theta + \frac{2\bar{x}\bar{y}}{a^2}\sin 2\theta$$
$$+ \left[3\left(\frac{\sigma_x^2-\sigma_y^2}{a^2}\right)+\left(\frac{\bar{x}^2-3\bar{y}^2}{a^2}\right)\right]\frac{\bar{x}}{a}cos3\theta + \left[3\left(\frac{\sigma_x^2-\sigma_y^2}{a^2}\right)+\left(\frac{3\bar{x}^2-\bar{y}^2}{a^2}\right)\right]\frac{\bar{y}}{a}sin3\theta]\} \tag{38}$$

which may be compared with (21), the case for a single line charge. We note that the purely geometrical part of the sextupole term in (21) and (38) differs from the result given in [6], which is in our notation:

$$E \approx E_\lambda \{1 + 2\,[\frac{\bar{x}}{a}\cos\theta + \frac{\bar{y}}{a}\sin\theta + \left(\frac{{\sigma_x}^2-{\sigma_y}^2}{a^2}+\frac{\bar{x}^2-\bar{y}^2}{a^2}\right)\cos 2\theta + \frac{2\bar{x}\bar{y}}{a^2}\sin 2\theta$$
$$+ \left[3\left(\frac{\sigma_x^2-\sigma_y^2}{a^2}\right)+\left(\frac{\bar{x}^2-\bar{y}^2}{a^2}\right)\right]\left(\frac{\bar{x}}{a}cos3\theta + \frac{\bar{y}}{a}sin3\theta\right)]\} \tag{39}$$

To investigate this difference, a beam was simulated as a multitude of line charges with Gaussian distributions in x and y. The field due to this beam as a function of angle around the perimeter of a circular pipe was calculated from (13), (38) and (39). It was found that (38) is always consistent with (13), whilst (39) is not, indicating an error in the derivation given in [6]. In the same reference, good agreement was nevertheless reported between theory and experimental data. This is possible since the authors based their measurements on scanning a beam in a BPM, keeping x zero whilst scanning in y and keeping y zero whilst scanning in x. Under these specific conditions, it may be seen that (38) and (39) become equivalent.

Proceeding with our derivation, we can again define a pickup geometry to sample the field distribution predicted by (38). We then use (26) and (27) to combine the button signals, yielding the results:

$$\Delta_X = \sqrt{2}\,\frac{x}{a}\left[1 - \left(3\frac{\sigma_x^2 - \sigma_y^2}{a^2} + \frac{x^2 - 3y^2}{a^2}\right)\right] \tag{40}$$

$$\Delta_Y = \sqrt{2}\,\frac{y}{a}\left[1 - \left(3\frac{\sigma_y^2 - \sigma_x^2}{a^2} + \frac{y^2 - 3x^2}{a^2}\right)\right] \tag{41}$$

3 Modelling the response of an elliptical BPM

In order to model the response of an elliptical BPM, we proceed in the same manner as before. First, the field to a single line charge may be calculated and some pickup geometry defined. Then the effect of a real beam may be calculated by superposition of the fields of many such line charges.

3.1 Conformal mapping for an elliptical pipe

The mapping $Z = K \sin W$ transforms line segments from $u = -\pi$ to $u = +\pi$ at $v = \pm ik$ in the plane W into an ellipse in the plane Z [12]. It follows that $W = \arcsin(Z/k)$ maps an ellipse in Z to the geometry of a parallel-plate capacitor in W, where k defines the aspect ratio of the ellipse in Z and the distance between the plates in W (Fig. 5). A value of $k = 0.5962$ was used to give the required aspect ratio and the absolute size of the ellipse scaled by a factor of 55.36.

A line charge placed within the ellipse in Z will appear within the capacitor in W. The image charges in W may be found by considering multiple reflections in the plates, the charge sign changing after each reflection. We obtain two infinite series of charges, corresponding to the first reflection occurring in one of the two plates. Each image charge may then be transformed back into Z.

We note that, as the aspect ratio of the ellipse in Z increases, the distance between the plates in W increases. For an aspect ratio approaching unity, the line charge appears in W close to one plate, whilst the other plate lies far away. Thus, only the first image charge is important and we retrieve the case of a circle.

3.2 Numerical calculation of the field

The calculation of the field at an elliptical pipe was implemented in FORTRAN code as follows. The parallel plate capacitor is drawn in the W plane and the conformal mapping used to calculate the sizes of the axes of the corresponding ellipse in Z. The equation of an ellipse in polar coordinates is:

$$r^2 = \frac{a^2 b^2}{a^2 \sin^2\theta + b^2 \cos^2\theta} \qquad (42)$$

where a is the semi-major axis and b the semi-minor axis. The angle is divided into 1000 steps between 0 and 2π; at each step the x and y coordinates of the perimeter of the ellipse are calculated. By representing the ellipse in Cartesian coordinates:

$$\frac{x^2}{a^2} + \frac{y^2}{b^2} = 1 \qquad (43)$$

the gradient of the contour dy/dx at each point is calculated. This allows a unit vector normal to the ellipse to be defined at each step.

The conformal mapping is then used as described previously to find the positions of the first twenty image charges in Z. The total electric field $E_\perp$ normal to the ellipse at any point P on the surface of the ellipse is found by summing over all the charges:

$$E_\perp = \left(\frac{\lambda}{2\pi\epsilon_0}\right) \sum_k \frac{1}{d_k}\, \hat{\mathbf{d}}_\mathbf{k} \cdot \hat{\mathbf{n}} \qquad (44)$$

where d_k is the distance between the kth charge and P, $\hat{\mathbf{d}}_\mathbf{k}$ is the unit vector in the direction from the kth charge to P and $\hat{\mathbf{n}}$ is the unit vector normal to the elliptical contour at P. One can also calculate the field tangential to the pipe, using $\hat{\mathbf{d}}_\mathbf{k} \times \hat{\mathbf{n}}$, as a cross-check; it should always tend towards zero since the pipe is conducting.

3.3 Response of the BPM to the field

The response of the BPM to the calculated field may now be obtained. The simplest model is to treat the BPM as having point electrodes at the centres of the buttons. The field at each point is calculated and the resulting signals combined according to (26) and (27).

During the development of the LEP BPMs, their response was characterised using an antenna mounted on an $x - y$ stage to provide a radio frequency signal representative of the beam [13]. The antenna was positioned at points on a grid of spacing 5 mm, scanning in x and y, and the BPM button signals measured at each point. This scenario was simulated using the computer model described above and the results compared with data [14]. The BPM output from the model is shown in Figs. 6 and 7.

The model predicts that the BPM response to beam position is sub-linear at large excursions in x and y. The response in a given direction is also affected by the beam position in the orthogonal direction. The overall features of the prediction are in agreement with the data and the absolute values agree to a level of $\sim 5\%$.

The geometry of the electrodes was refined by representing each button as a straight line of length equal to the button diameter. The button signal was obtained by calculating the field at 100 points along the line. For this model, the agreement between data and the antenna measurement was better than 2%. In the experimental situation, the values of $K_H = 26.56$ and $K_V = 38.28$ were chosen so that the position indicated by the BPM was correct at the points (5 mm,0) and (0,5 mm) respectively. Simulating the same situation gave $K_H = 26.68$ $K_V = 37.70$.

3.4 Response of en elliptical BPM to a Gaussian beam

Once the field due to a single line charge within a conducting boundary has been found, it is simple to simulate a realistic beam by superposition of many line charges. The CERN library function RNORMX was used to generate 5000 random numbers with a Gaussian distribution for each simulation. A schematic of the model appears in Fig. 8, where the first two image charge distributions are shown for a beam with a small offset in x.

For each line charge within the beam, the image charge positions are calculated and used to obtain the field at each point on the pipe. The fields due to all such line charges are then added up. The effect of changing beam dimensions on BPM response for point buttons is shown in Fig. 9. At the Spectrometer, the beam width is much larger in the horizontal plane than in the vertical and so only the effect of σ_x variation is included in the figure. The beam was taken to lie at a position of (1 mm,0) and the horizontal correction calculated as a function of varying σ_x. The vertical correction was calculated similarly, for a beam at (0,1 mm). The plot symbols represent the simulation results; the uppermost and lowest curves are parabolae fittted through the simulated points. For the case of a circular beam pipe, the plot symbols are again the simulated points, whilst the parabola is that predicted by the analytical model. The elliptical BPM is less sensitive to beam size effects in the horizontal plane than in the vertical.

The button geometry also affects the response of the BPM to beam size. Fig. 10 shows the effect of beam size calculated for the more realistic button model described above. The effect of button dimensions is more marked in the vertical plane than in the horizontal.

4 The Effect of BPM nonlinearities on the Spectrometer

It is required that the change in bending angle be determined as the machine is ramped from a polarisation energy (taken to be 45.0 GeV) to the physics energy (taken to be 94.5 GeV). In order to minimise the BPM nonlinearities, which scale with beam displacement, it is necessary to steer the beam as close to the nominal path as possible. The beam trajectory should therefore be corrected before and after the ramp to high energy. However, the accuracy of such a correction is not absolute, so that the beam position and/or angle may not be the same at the two energies. In addition, physical misalignment of the BPM blocks with respect to each other may introduce systematic errors on the change in bending angle.

The beam size varies along the spectrometer according to:

$$\sigma_x = \sqrt{\varepsilon_x \beta_x(s) + \sigma_\delta^2 D^2(s)} \tag{45}$$

in x and similarly in y, where s is the longitudinal coordinate, ε the emittance, $\beta(s)$ the betatron function and $D(s)$ the dispersion in the given plane. The value of $\sigma_\delta = \sigma_E/E$ was taken to be $1.549\times10^{-3}\,E/100\,\mathrm{GeV}$. The design horizontal emittance was taken to be 8.5 nm at 45.0 GeV and 38.3 nm at 94.5 GeV, with a vertical/horizontal emittance ratio of 1%. The β functions and dispersion are shown for the 101/45 optics in Figs. 11 and 12, in which the plot symbols represent the Spectrometer BPM locations. As a result of the change in beam size, each BPM records a different error in the beam position. This introduces an error on the angle determined, which is different before and after the ramp as the emittance changes and which becomes larger with increasing beam displacement.

4.1 Errors introduced by parallel orbit changes

The beam size was calculated at the two outermost BPMs in each Spectrometer arm. Fig. 13 shows the absolute error in each of these BPMs as a function of beam displacement, calculated for 94.5 GeV. The difference in the reading between BPM6 and BPM4 leads to a trajectory parallel to the nominal path being reconstructed as an angled track. The same effect is apparent for BPM1 and BPM3. The error is proportional to σ^2, varying roughly linearly with β, so that the overall effect is that the beam appears to be rotated in each arm. However, the rotations measured in the two arms tend to cancel, leaving only a small error on the measured bending angle itself.

Fig. 14 shows the fractional error on the bending angle as a function of orbit correction. At each simulated point, the measured bending angle was calculated at 45.6 GeV and 95.4 GeV for a beam at the nominal angle. The beam was assumed to lie at a distance $-\delta x$ from the BPM centres at the lower energy, drifting to $+\delta x$ at the higher. The fractional error was taken to be the sum of the errors of the two individual angle reconstructions, divided by the nominal bending angle of 3.75 mrad. It can be seen from the figure that the error becomes negligible for orbit corrections better than $\sim$500 μm; at LEP, it is possible to steer the beam with a reproducibility approaching $\pm$50 μm [15].

4.2 Errors introduced by beam angle changes

Any beam movement may be considered as a superposition of a parallel drift and a rotation. The effect of a change in beam angle during the ramp was investigated by rotating the beam about the centre of the Spectrometer magnet from an angle $-\delta\theta$ to the nominal path at 45.6 GeV to $+\delta\theta$ at 94.5 GeV. The individual BPM readings were calculated as before and used to find the error on the reconstructed angle. The total fractional error was again taken as the sum of the errors at low and high energy divided by the nominal bending angle. The error is shown as a function of beam angular deviation in Fig. 15. That the reproducibility in the end BPMs of the steered beam is 50 μm leads to control of the beam angular deviation around the 15 μrad level. The overall fractional error is in this case similar to that due to the magnet mapping.

4.3 Errors introduced by BPM misalignment

If the BPMs are offset with respect to each other, a track fitted through the Spectrometer will result in the bending angle being calculated incorrectly. However, if the pickups were linear, an error would not be introduced on the change in the bending angle. It is again the change in beam size during the ramp that introduces such an error, shown as a function of BPM offset in Fig. 16.

For the simulation, it was assumed that the innermost BPMs were displaced away from the centre of the LEP ring and the outermost BPMs displaced towards the centre by an equal amount. This is a worst case scenario. The alignment errors of the BPM blocks are expected to be randomly distributed with an RMS of $\sim 100\,\mu$m, so that a realistic value for the correlated error is $50\,\mu$m, making the approximation that the errors associated with each pickup are equal. The beam was assumed to lie at -100μm from the pickup centres at 45.0 GeV, drifting to +100μm after the ramp to 94.5 GeV.

From Fig. 16, it can be seen that, as long as the BPMs are aligned to the design tolerance, the systematic error due to BPM offsets will be acceptably small. The offset from zero of the graph is due to the orbit drift included in the simulation; larger orbit drifts have the effect of translating the plot further up the y axis.

5 Summary and Conclusions

The response of a circular BPM to an infinite line charge has been calculated analytically and used to derive the effect of a realistic beam size, under the assumption that the transverse charge distributions are Gaussian. Possible high-frequency and bunch length effects have been neglected. Based on this formalism, a numerical calculation was implemented of the response of the LEP elliptical BPMs.

The nonlinearities in the BPM response due to geometrical and beam size effects were used to calculate the errors introduced on the bending angle in the LEP Spectrometer as the machine is ramped from polarisation to physics energies. It has been shown that the beam steering which is routinely achievable is sufficient to suppress errors from parallel or angular beam drifts during the ramp. The alignment of the pickups themselves is also important if systematic errors are not to be introduced; adequate alignment precision is achievable.

We also note that the nonlinearities might be used to advantage if the linearity and resolution of the electronics is sufficient. From Equations 40 and 41, if it were possible to scan the BPMs relative to the beam, one could in principle determine whether the BPM was centred on the beam. If the beam were held at a constant, large y and the BPM scanned in x, the BPM response would be parabolic in form. The minimum of the parabola would indicate when the BPM was centred, independent of electronic offsets. Further, the beam size could be extracted from the y intercept of the parabola, if the electronics chain was calibrated with sufficient accuracy. Although the LEP pickup geometry is not optimal for beam size measurements, it is possible to envisage an emittance monitor based on the same principle, perhaps using a dedicated pickup design.

6 Acknowledgements

I would like to thank Ralph Assmann for bringing this problem to my attention and for providing the data from which the beam size is derived. Bernd Dehning, Jan Prochnow and Rudolf Bossart are acknowledged for several helpful discussions. I am grateful to Massimo Placidi for his careful reading of the manuscript.

References

[1] L.Arnaudon et al., Accurate Determination of the LEP Beam Energy by Resonant Depolarization, Z. Phys. C66, 45-62 (1995)

[2] M.Placidi, Beam Energy Measurement Possibilities at LEP2, proceedings of the 6th LEP Performance Workshop, Chamonix CERN-SL-96-05-DI (1996)

[3] See for example M.Placidi in the proceedings of the 8th LEP Performance Workshop, Chamonix CERN-SL-98-006-DI (1998)

[4] F.Roncarolo, Diploma thesis, Politecnico di Milano (2000)

[5] Bergoz Instrumentation, 01630 St. Genis Pouilly, France

[6] R.H.Miller et al., Nonintercepting Emittance Monitor, 12th. Int. Conf. on High Energy Accelerators, Batavia, Illinois (1983)

[7] R.Bossart, Coaxial Cavity as Position Monitor of Ultrahigh Frequency Beams, CERN Lab II-CO/BM/Int.Note/RB/75-13 (1975)

[8] C.Bovet, Solution d'un Probleme Electrostatique, CERN MPS/DL Int.65-13 (1965)

[9] R.T.Avery, A.Faltens and E.C.Hartwig, Non-Intercepting Monitor of Beam Current and Position, IEEE Trans. Nucl. Sci. NS-18, 920 (1971)

[10] I.S.Gradshteyn and I.M.Ryzhik, Table of Integrals, Series and Products, Academic Press.

[11] S.Wolfram, The Mathematica Book, Cambridge University Press

[12] Z.Nehari, Conformal Mapping, McGraw-Hill (1952)

[13] J.Borer, C.Bovet, D.Cocq, Algorithmes de Linearisation des Pick-Ups, LEP Note 582 (1989)

[14] J.Borer, D.Cocq, private communication

[15] J.Wenninger, private communication

Fig.1 Layout of the Spectrometer

Fig.2 A Spectrometer BPM

Fig.3 Conformal mapping for circular pipe

Fig.4 Calculation of the total field around a circular pipe

Fig.5 Conformal mapping for an elliptical pipe

Fig.6 Response of an elliptical BPM: x output

Fig.7 Response of an elliptical BPM: y output

Fig.8 Model of an elliptical BPM with a Gaussian beam

Fig.9 Corrections due to beam size for a circular and an elliptical vacuum chamber (see text for details)

Fig.10 Corrections due to beam size for a an elliptical vacuum chamber and different button geometries

Fig.11 Values of the beta functions at the Spectrometer (101/45 optics)

Fig.12 Dispersion at the Spectrometer (101/45 optics)

Fig.13 Absolute errors at the BPMs

Fig.14 Fractional error on the bending angle due to orbit parallel correction error

Fig.15 Fractional error on the bending angle due to orbit angular correction error

Fig.16 Fractional error on the bending angle due to BPM misalignment

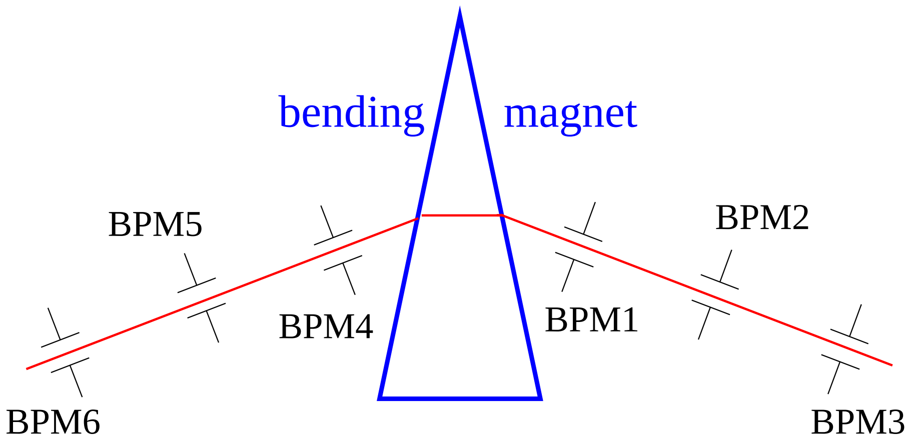

Figure 1:

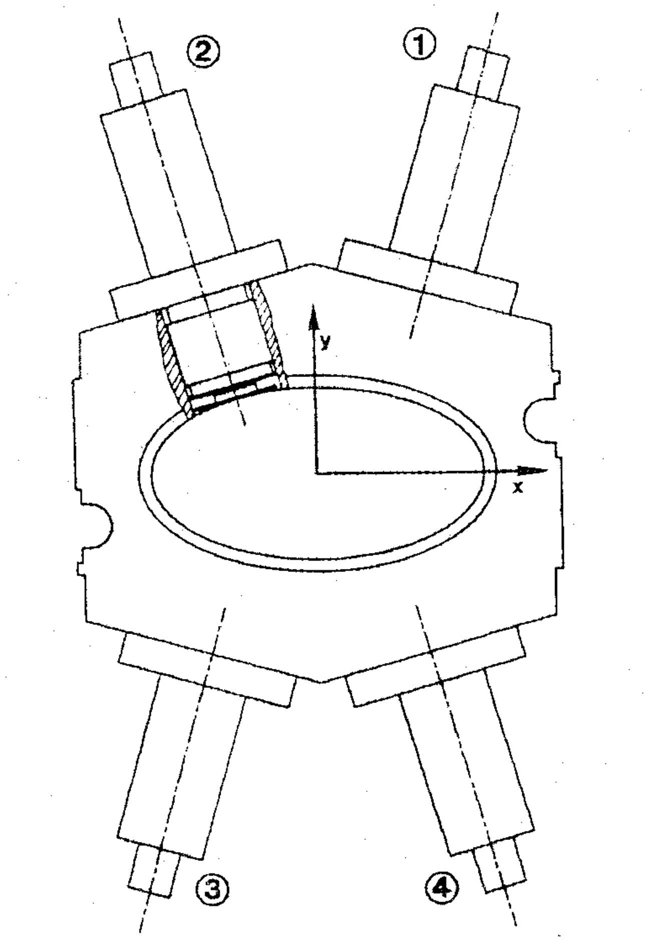

Figure 2:

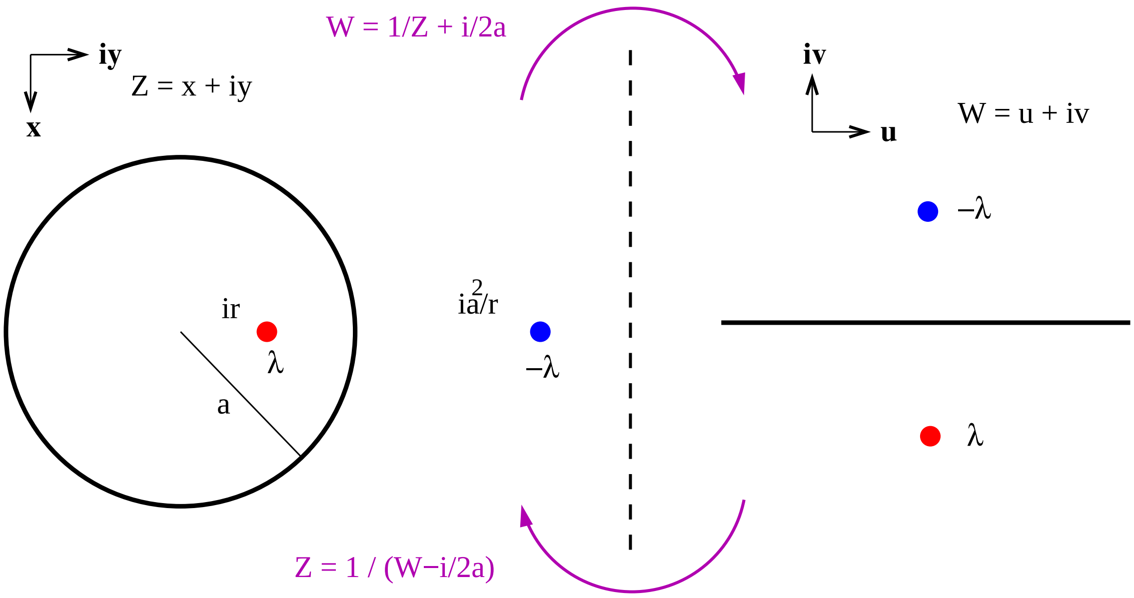

Figure 3:

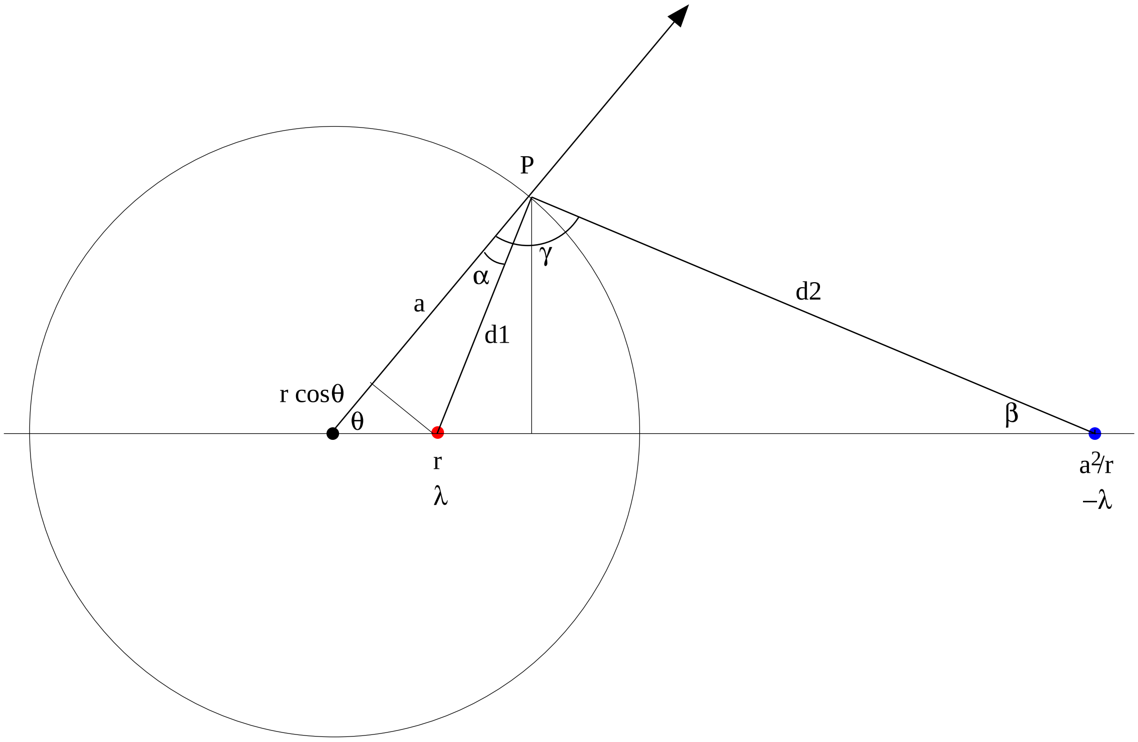

Figure 4:

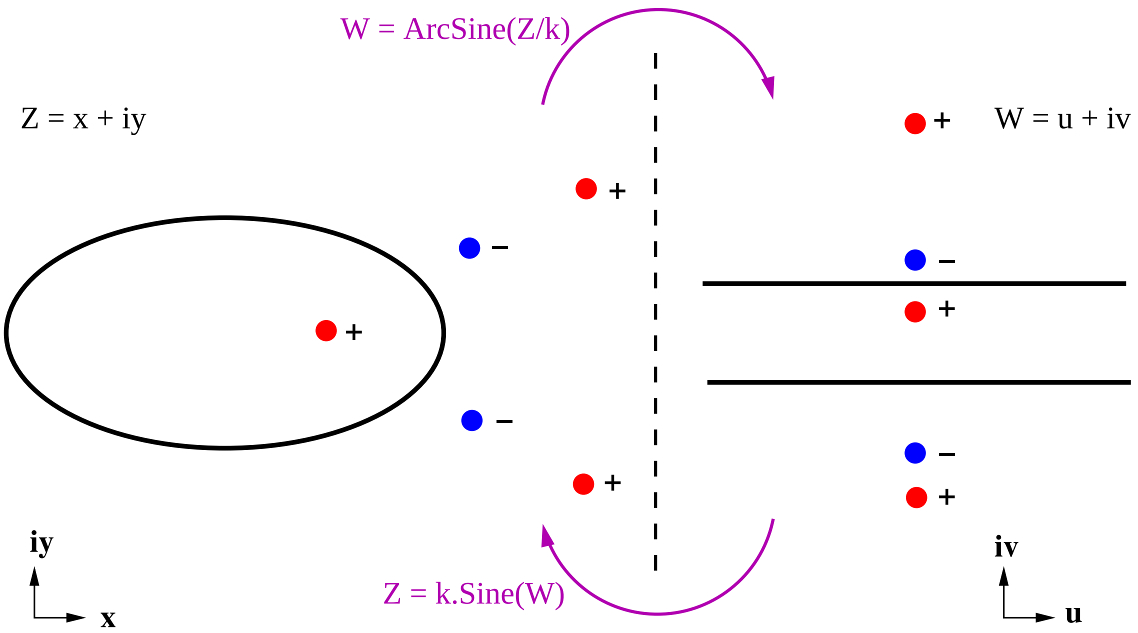

Figure 5:

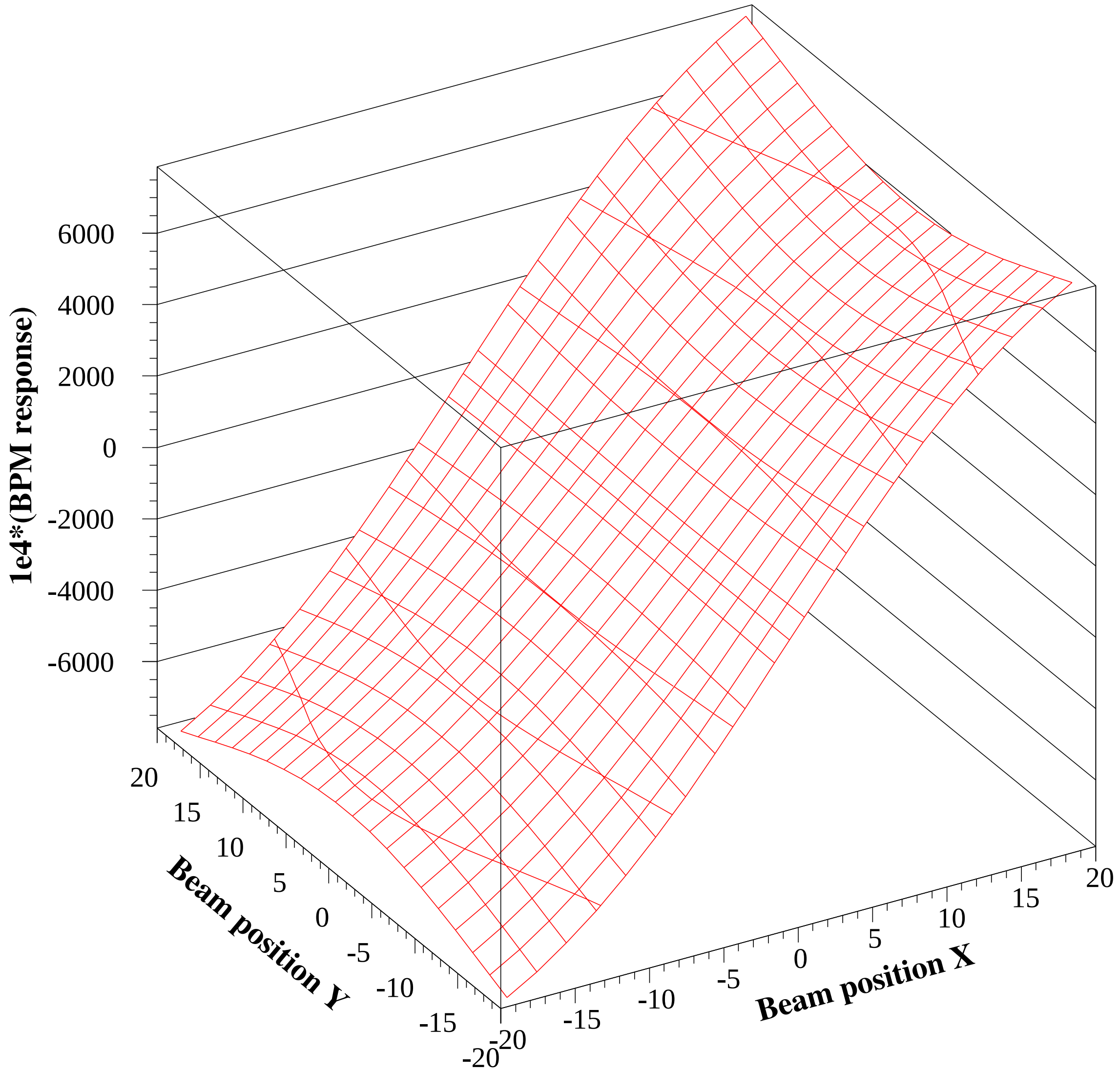

1e4*(BPM response)
6000
4000
2000
0
-2000
-4000
-6000
Beam position Y
20
15
10
5
0
-5
-10
-15
-20
Beam position X
-20
-15
-10
-5
0
5
10
15
20

Figure 6:

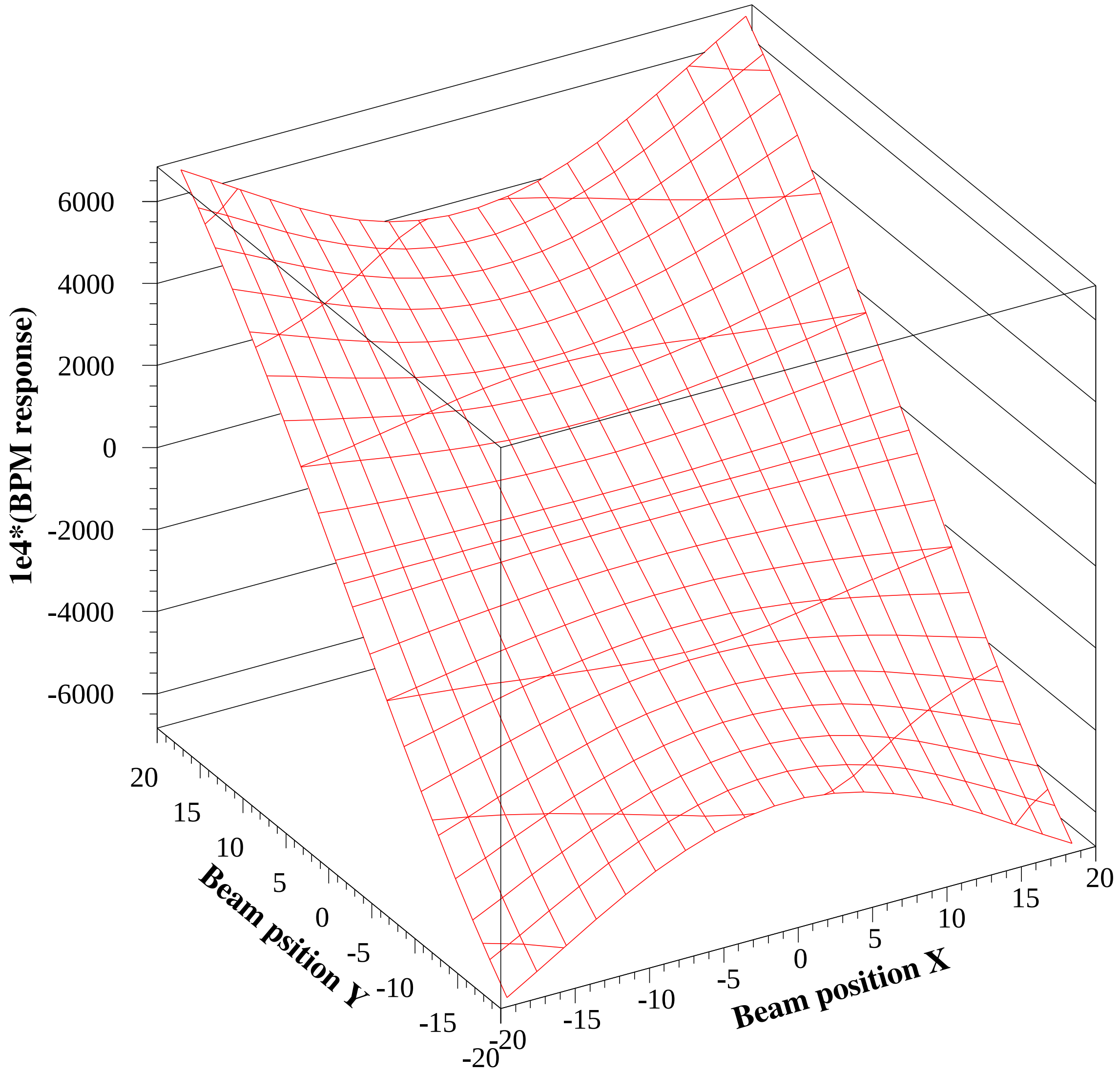
1e4*(BPM response)
6000
4000
2000
0
-2000
-4000
-6000
Beam psition Y
20
15
10
5
0
-5
-10
-15
-20
Beam position X
-20
-15
-10
-5
0
5
10
15
20

Figure 7:

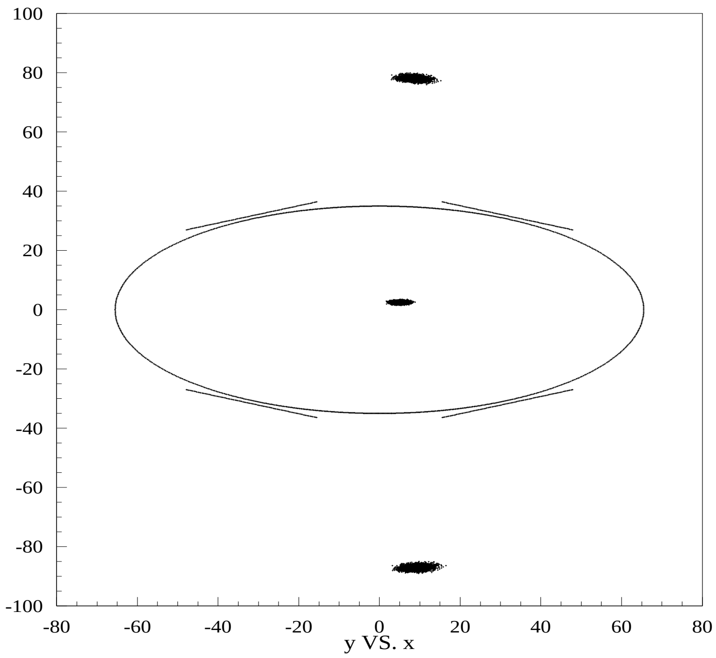

Figure 8:

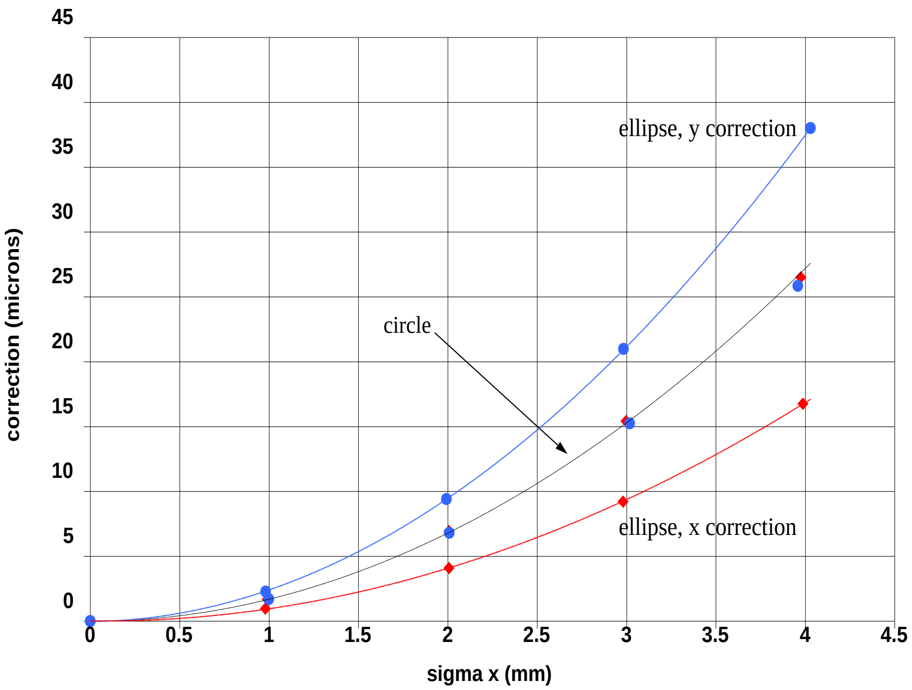

Figure 9:

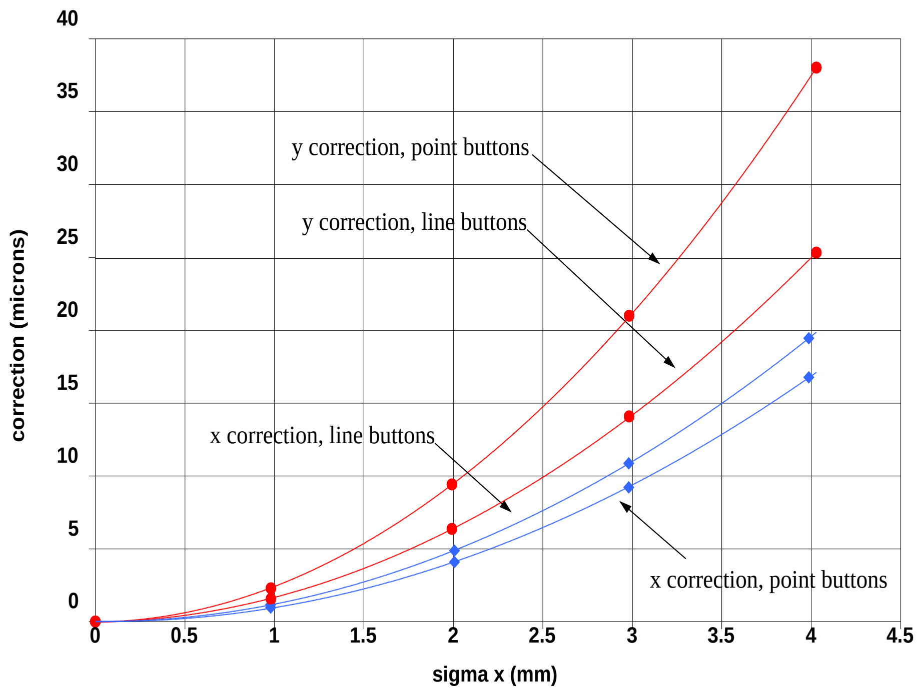

Figure 10:

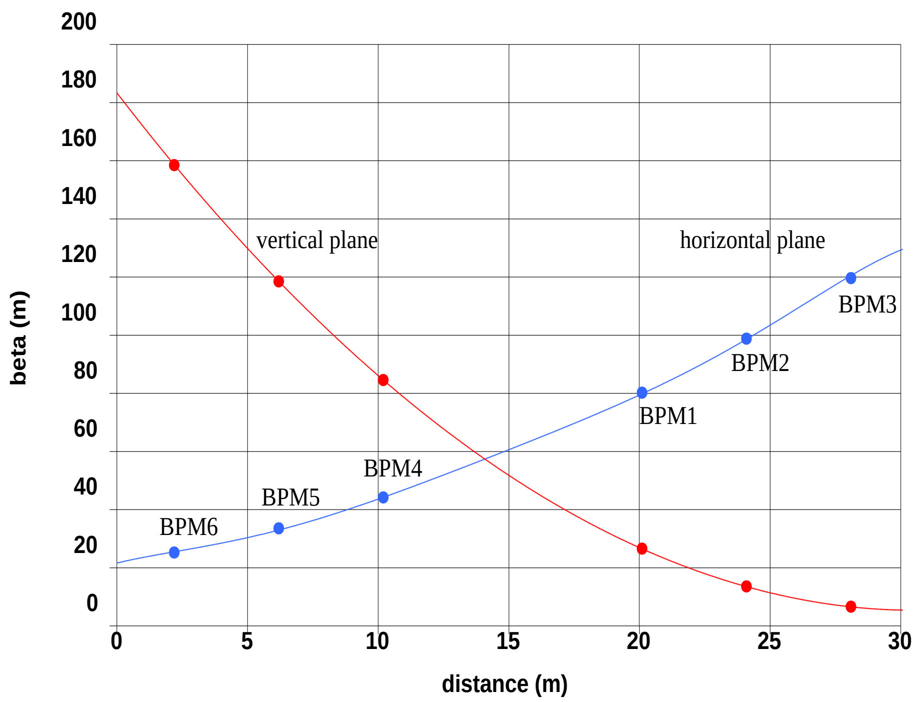

Figure 11:

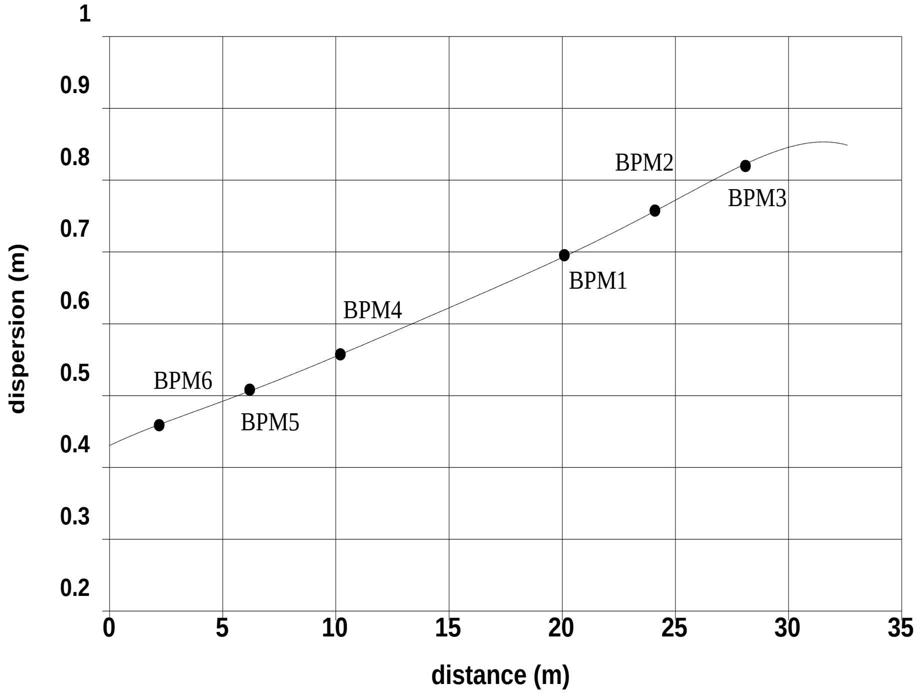

Figure 12:

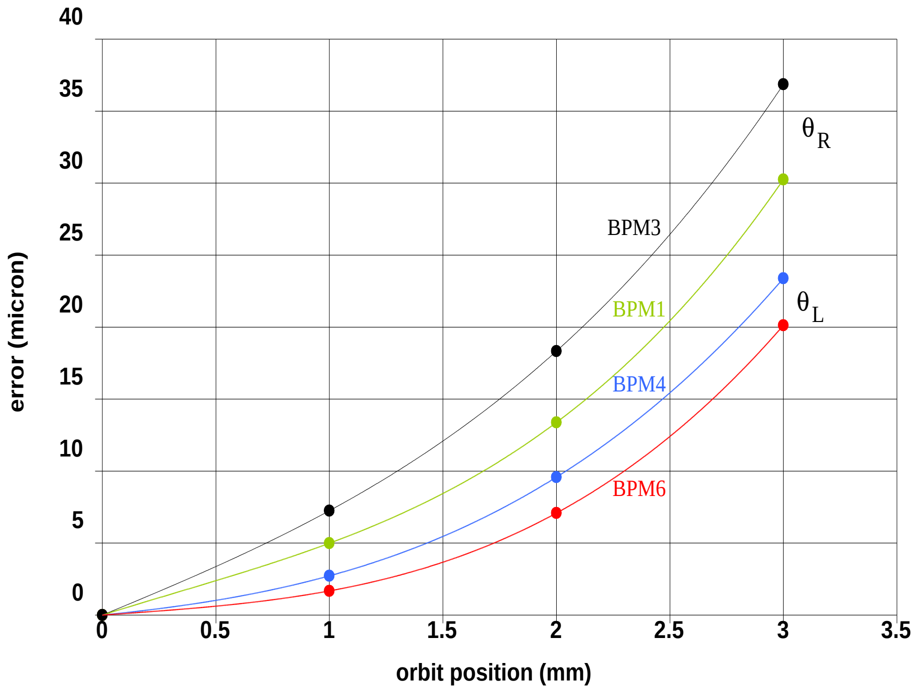

Figure 13:

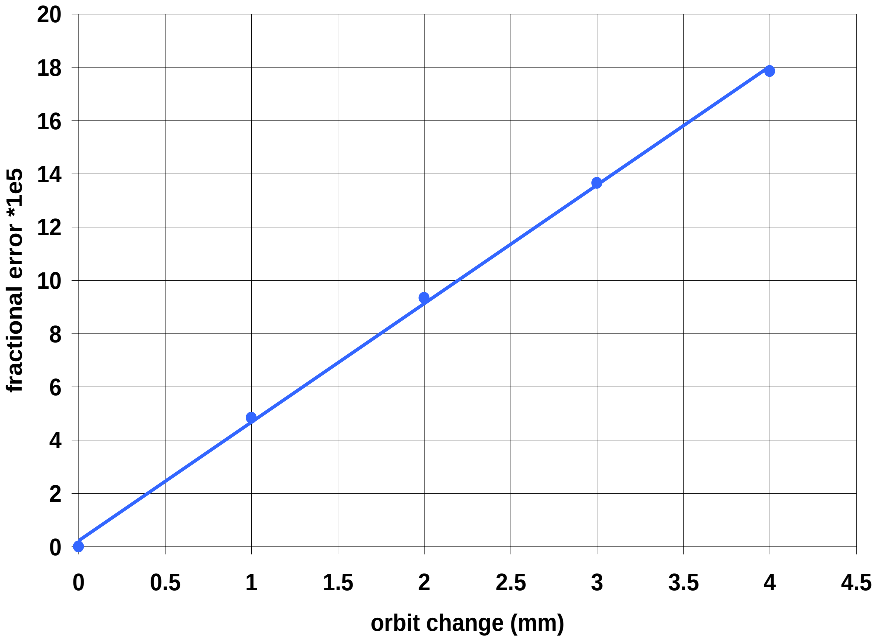

Figure 14:

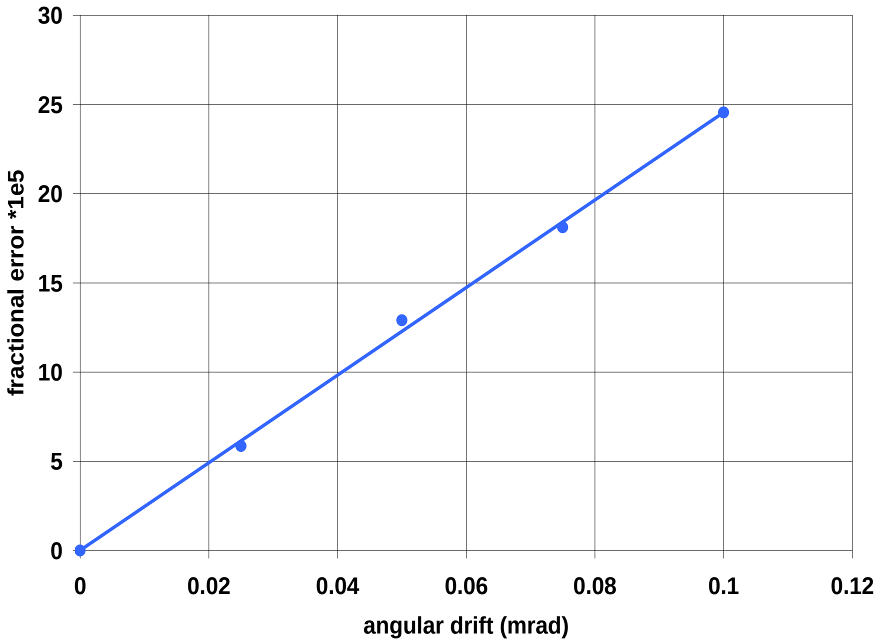

Figure 15:

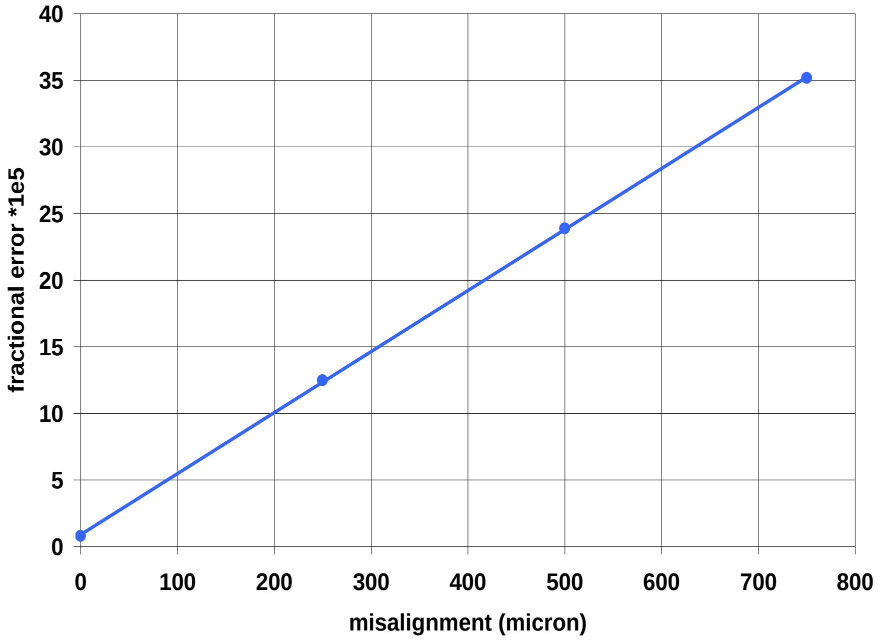

40
35
30
25
20
15
10
5
0
fractional error *1e5
0
100
200
300
400
500
600
700
800
misalignment (micron)

Figure 16: